Int. J. Electrochem. Sci., 14 **(2019)** 929 – 942, doi: 10.20964/2019.01.79

International Journal of
ELECTROCHEMICAL
SCIENCE
www.electrochemsci.org

Effect of Ni and Cu Substitution on the Crystal Structure, Morphology and Electrochemical Performance of Spinel $LiMn_2O_4$

Azhar Iqbal[1,*], *Abdul Majeed Khan*[2,*], *Tao Wang*[1], *Daocong Li*[1], *Yuxian Gao*[1]

[1]Institute of Engineering Research, Hefei Guoxuan High-Tech Power Energy Co., Ltd, Hefei, 230011, P. R. China.
[2]General Studies Department, Jubail Industrial College, Jubail Industrial City 31961, Kingdom of Saudi Arabia.
[*]E-mail: aiqbalchemist@yahoo.com, fahmigul@yahoo.com

Received: 24 September 2018 / *Accepted:* 28 October 2018 / *Published:* 30 November 2018

Ni and Cu bi-metal doping of spinel $LiMn_2O_4$ materials are investigated by characterizing the as prepared materials by XRD, FTIR, SEM, TEM, CV, Charge/discharge measurements and electrochemial impedance spectroscopy (EIS). Although, Ni and Cu doping decreased the initial discharge capacity, the optimized composition such as $LiNi_{0.01}Cu_{0.01}Mn_{1.98}O_4$ demonstrates good capacity retention after prolonged charge/ discharge cycling and high rate capability. The observed enhanced electrochemical performance of Ni-Cu bi-metal doped samples may be attributed to the suppression of the strucutral changes along with improved lithium-ion kinetics during charge/ discharge process.

Keywords: Electrochemical performance; Metalsdoped Li-Ion Batteries;

1. INTRODUCTION

High-power and high-energy rechargeable batteries based on earth-abundant materials are important for mobile and stationary energy storage applications. Among various energy storage systems, lithium-ion batteries (LIBs) are the most popular and widely used systems due to advantages such as high voltage, high energy density, long life span, low self-discharge and lack of memory effect [1-4]. Several excellent reviews have very well explained the importance of rechargeable lithium batteries in portable electronics and their potential for electrifying transportation and renewable power station [5-7]. The development of LIBs with high energy and power densities as well as excellent cycling stability has become crucial issue with ever increasing demand for high energy storage devices [8-10]. As an essential component, electrode material plays a decisive role in pursuing high pursuing high performance lithium-ion batteries. In commercial LIBs, $LiCoO_2$ is mostly used as the cathode material. However, the high toxicity, high cost and limited resources of cobalt have motivated extensive efforts to develop electrochemically active cathode materials. Among these materials, spinel $LiMn_2O_4$ with high theoretical capacity (148 mAh g^{-1}) has gained much attention because of its low manufacturing cost, non-toxicity, relative abundance and environmental friendliness [11-15]. The relative stability (thermodynamically speaking) of the delithiated structure of spinel $LiMn_2O_4$ results in fast charging compared to the commercially used layered $LiCoO_2$, which undergoes unwanted structural changes in an overcharged state that ultimately lead to poor battery performance [16]. However, the practical application of the bulk $LiMn_2O_4$ could not satisfy the high power requirements because of kinetic limitations such as low ionic and electronic conductivities, small lithium diffusion coefficient. The poor cycling performance is also caused by the Jahn-Teller distortion and Mn dissolution due to disproportionation reaction [17-20]. Until now, the most important factor responsible for structural degradation that results in capacity fading in spinel $LiMn_2O_4$ is the Jahn-Teller distortion effect. One effective approach to improve the structural stability and combat the capacity fading is to increase the average Mn oxidation state at the end of discharge by doping with appropriate metal cations (e.g., Li, Ni, Cu, Zn, Co, Cr, Al, Mg) [21-23]. The enhanced structural stability and the weakened Jahn-Teller distortion effect can further improve the cycle performance of the spinel $LiMn_2O_4$. Furthermore, cation doping has been reported to alter the mechanism and numbers of different phases that co-exist during charging, thus affecting the performance of the material over repeated charge/ discharge cycling [23]. For example, Ding and co-worker have reported the synthesis of Al doped $LiMn_2O_4$ that exhibited better cycling performance both at room and high temperature [24]. Multiple cation doping has also been found effective for the better electrochemical charge/discharge cycling and high rate performance [25, 26].

In the present work, we have investigated the effect of bi-metal (Ni and Cu) doping on the crystal structure, morphology and electrochemical properties of $LiMn_2O_4$. As expected, the as-synthesized Ni-Cu bi-metal doped (hereafter denoted as NC-LMO) cathode materials have shown markedly enhanced cycling stability and rate performance than the pure $LiMn_2O_4$.

2. EXPERIMENTAL DETAILS

All reagents used in the experimental work were of analytical grade and were directly use without any further purification. High purity manganese acetate ($Mn(CH_3COO)_2$; Aldrich, 98%), lithium acetate ($Li(CH_3COO)$; Aldrich, 99.95%), nickel nitrate hexahydrate ($Ni(NO_3)_2 \cdot 6H_2O$; Aldrich, 99.99%), copper(II)acetate($Cu(OOCCH_3)_2$; Alfa Aesar, 99.999%).

2.1. Experimental

Citric acid assisted sol-gel method was used for the preparation of pure $LiMn_2O_4$ and Ni-Cu bi-metal doped samples ($Li[Ni_xCu_yMn_{2-x-y}]O_4$) (where, x = y = 0.01-0.05). In a typical sol-gel process for the preparation of doped samples, stoichiometric amount of lithium acetate, manganese acetate, nickel acetate nonahydrate, copper acetate and citric acid were separately dissolved in 50 mL de-ionized water.

These solutions were mixed together to get a final solution having a total volume of 250 mL. Citric acid to metal ions molar ratio was kept at 1. To maintain the pH value at 6.0, ammonium hydroxide was slowly added to this solution with constant stirring. The resultant solution was evaporated at 80°C while being mechanically stirred with a magnetic stirrer for 5 h until a gel was obtained. The gel precursor obtained was dried overnight at 120 °C to remove moisture. The resulting powder sample was initially calcined at 400 °C for 5 h and then at 750 °C for 10 h at a heating rate of 5 °C/ min to obtain $LiNi_xCu_yMn_{2-x-y}O_4$ (NC-LMO). By contrast, pure $LiMn_2O_4$ was prepared with a similar procedure only without the addition of the dopant cations.

2.2. Characterization

The as prepared products were characterized by X-ray diffraction (XRD, Panalytical X'Pert-Pro MPD), thermo gravimetric analysis (TGA/DTA, PerkinElmer Diamond), scanning electron microscopy (SEM, Hitachi S-4800), Transmission electron microscopy (TEM, Tecnai G20 S-TWIN),) and Fourier transform infrared spectroscopy (FT-IR, PE2000). Inductively coupled plasma optical emission spectrometry (ICP-OES, Perkin Elmer Optima 5300DV) was used to determine the chemical composition of the prepared materials.

2.3. Electrochemical measurements

Electrochemical properties of the synthesized materials were measured by charging/ discharging test. Half cells using lithium foil as a reference electrode were assembled with CR2032 coin-type cells in the glove-box. To make slurry, 80 wt % of the active material, 10 wt% acetylene black and 10 wt% polyvinylidene fluoride (PVDF) were mixed together in N-methyl-2-pyrrolidone (NMP). The slurry was then casted onto an Al foil current collector and dried at 120 °C for 12 h under vacuum. Then circular cathode discs were punched from the Al foil. The punched cathodes were weighed to determine the amount of active materials before being loaded into coin-type cells. For all the electrochemical measurements, 1.0 M $LiPF_6$ dissolved in ethylene carbonate (EC)/dimethyl carbonate (DMC) was used as the electrolyte. Charge/ discharge measurements were performed at different current densities using CT2001A LAND battery tester. CHI 660C electrochemical workstation was used for cyclic voltammetry (CV) and electrochemical impedance spectroscopy (EIS) measurements.

3. RESULTS AND DISCUSSION

Ni-Cu bimetal doped $LiMn_2O_4$ (NC-LMO) materials were synthesized by a simple sol-gel method using citric acid as a chelating agent. The morphology and structure of the pure and NC-LMO were examined by field emission scanning electron microscopy (FESEM).

Figure 1, shows that the pure $LiMn_2O_4$ is composed of highly aggregated particles while low agglomeration of the particles is obtained for NC-LMO. Furthermore, the particles of NC-LMO samples are well separated and grow in size as the dopant level increases; this observation is in good agreement with XRD results shown in 1.To provide further insight about the structure and morphology of the prepared samples, transmission electron microscopy (TEM) was performed as shown in Figure 2. In good agreement with the SEM results, TEM images show that NC-LMO samples are composed of particles that illustrate well-separated grain boundaries. The mean particle size of the NC-LMO samples ranged from about 70 nm to 150 nm. High-resolution TEM image shown in the inset of Figure 2b. for the doped sample $LiNi_{0.01}Cr_{0.01}Mn_{1.98}O_4$ depicts a set of lattice fringes with an interplanar spacing of 0.47 nm which corresponds to the (111) crystal planes of the spinel $LiMn_2O_4$ phase [27]. This clearly shows the highly crystalline nature of the prepared materials with no obvious imperfection.

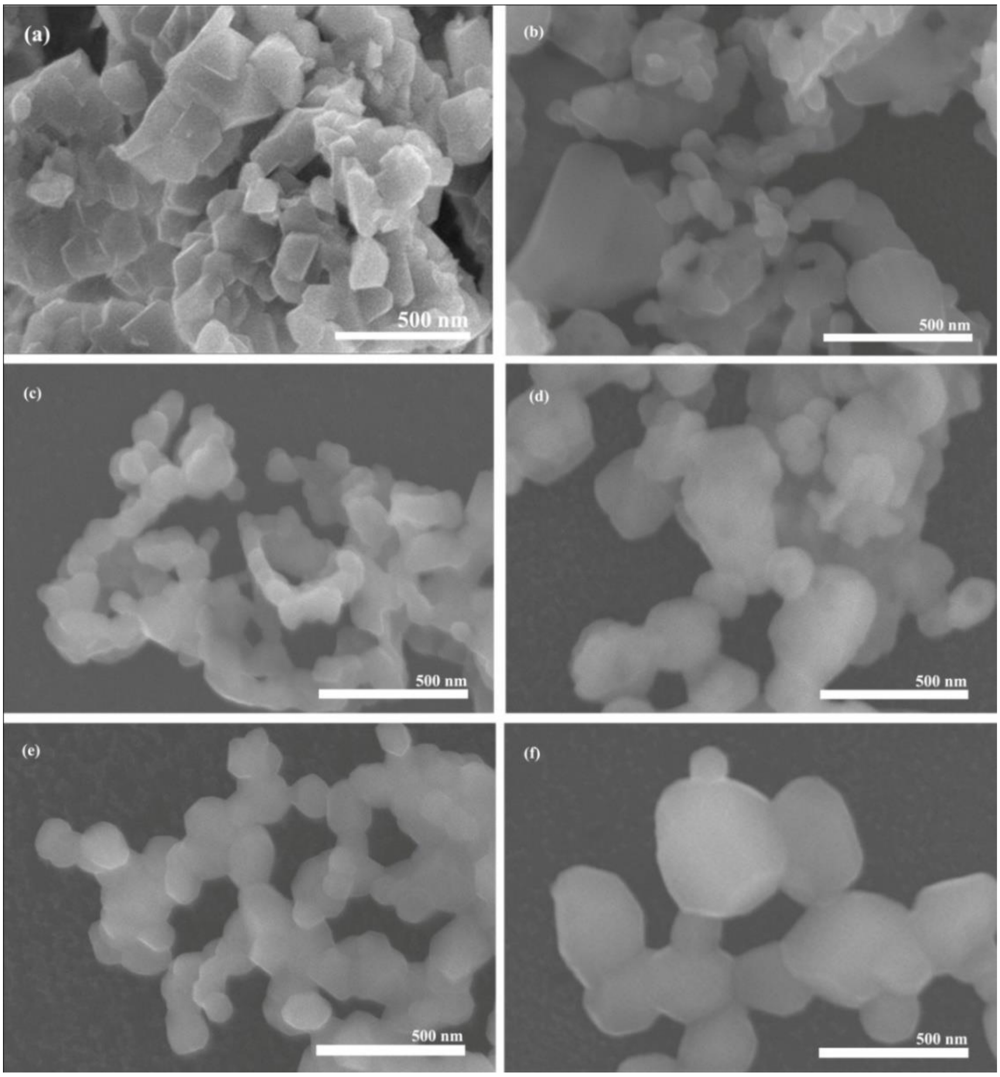

Figure 1. SEM images of (a) $LiMn_2O_4$ (b) $LiNi_{0.01}Cu_{0.01}Mn_{1.98}O_4$ (c) $LiNi_{0.02}Cu_{0.02}Mn_{1.96}O_4$ (d) $LiNi_{0.03}Cu_{0.03}Mn_{1.94}O_4$ (e) $LiNi_{0.04}Cu_{0.04}Mn_{1.92}O_4$ (f) $LiNi_{0.05}Cu_{0.05}Mn_{1.90}O_4$.

Table 1. Lattice parameter and unit cell volume of the pure and Ni-Cu bi-metal doped samples.

S. No	Sample	Lattice constant *'a'* (Å)	Unit cell Volume (Å^3)
1	$LiMn_2O_4$	8.2478	561.06

2	$LiNi_{0.01}Cu_{0.01}Mn_{1.98}O_4$	8.1658	544.49
3	$LiNi_{0.02}Cu_{0.02}Mn_{1.96}O_4$	8.1673	544.79
4	$LiNi_{0.03}Cu_{0.03}Mn_{1.94}O_4$	8.1681	544.95
5	$LiNi_{0.04}Cu_{0.04}Mn_{1.92}O_4$	8.1892	549.19
6	$LiNi_{0.05}Cu_{0.05}Mn_{1.90}O_4$	8.1897	549.29

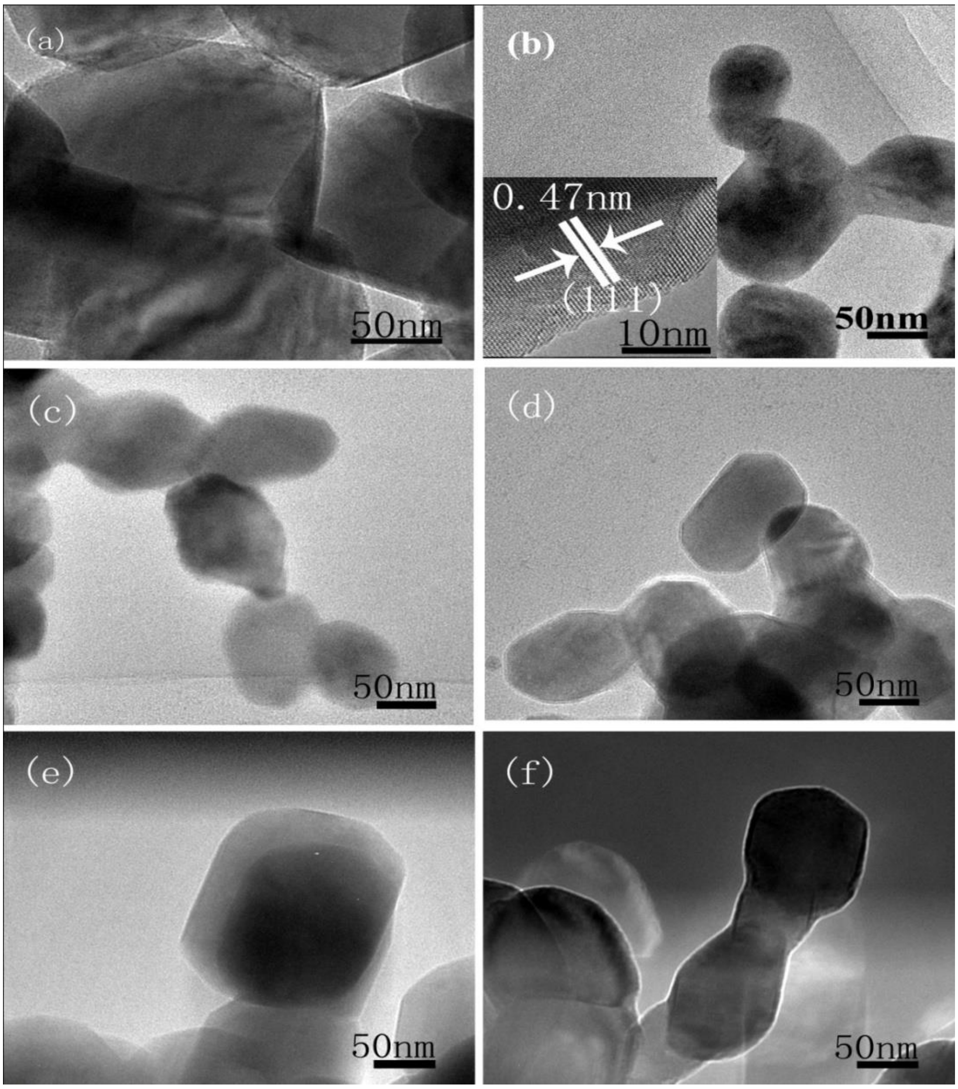

Figure 2. TEM images of (a) $LiMn_2O_4$ (b) $LiNi_{0.01}Cu_{0.01}Mn_{1.98}O_4$ (c) $LiNi_{0.02}Cu_{0.02}Mn_{1.96}O_4$ (d) $LiNi_{0.03}Cu_{0.03}Mn_{1.94}O_4$ (e) $LiNi_{0.04}Cu_{0.04}Mn_{1.92}O_4$ (f) $LiNi_{0.05}Cu_{0.05}Mn_{1.90}O_4$.

The phase structures of the pure and NC-LMO samples were examined by powder XRD measurement. All the diffraction peaks depicted in Figure 33, can be assigned to a well-crystalline spinel $LiMn_2O_4$ (JCPDS No. 35-0782) with space group *Fd3m* where Li-ions occupy the tetrahedral (8a) sites while Mn and the doped metal ions (Ni and Cu) reside in the octahedral (16d) sites [28]. No other characteristic peaks from the impurity phases are detected from XRD measurement.

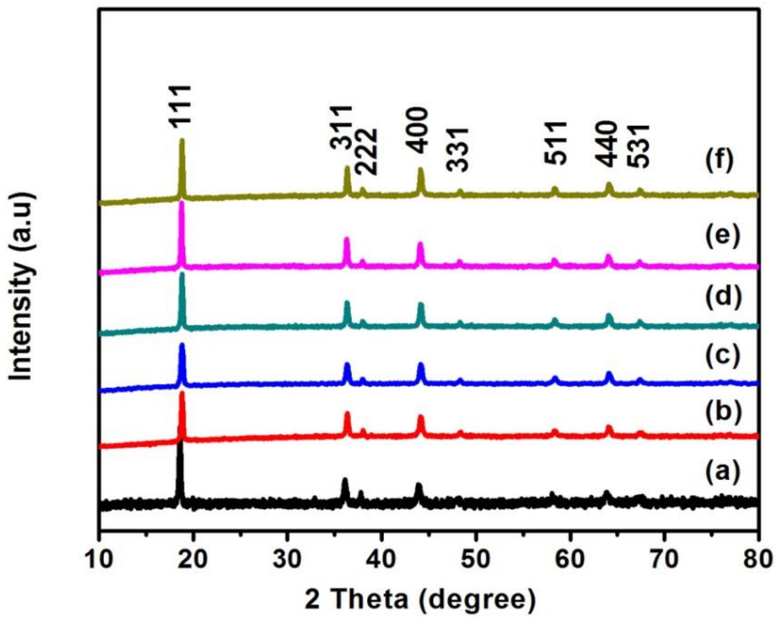

Figure 3. XRD patterns of (a) $LiMn_2O_4$ (b) $LiNi_{0.01}Cu_{0.01}Mn_{1.98}O_4$ (c) $LiNi_{0.02}Cu_{0.02}Mn_{1.96}O_4$ (d) $LiNi_{0.03}Cu_{0.03}Mn_{1.94}O_4$ (e) $LiNi_{0.04}Cu_{0.04}Mn_{1.92}O_4$ (f) $LiNi_{0.05}Cu_{0.05}Mn_{1.90}O_4$.

Furthermore,

Table 1 shows the lattice constant and unit cell volume calculated from XRD data for all the prepared samples. A decrease in the lattice parameters is observed. For NC-LMO samples, the initial decrease in particle size may be attributed to the fact that when minor amount of Cu^{2+} ions is present, most of the Cu^{2+} ions will reside in the tetrahedral sites of the spinel $LiMn_2O_4$, thus resulting in smaller lattice parameter than the pure spinel $LiMn_2O_4$. As it has already been reported [29] that the effective ionic radius of tetrahedrally coordinated Cu^{2+} ion (0.57 Å) is rather smaller than Li^+ ion (0.59 Å). Upon increasing the amount of Cu in the spinel framework, Cu^{2+} ions will also tend to occupy the octahedral sites that were initially engaged by the Mn^{3+} ions. Thus, the particle size get increased as the effective ionic radius of the octahedrally coordinated Cu^{2+} ion (0.73 Å) is larger than Mn^{3+} ion (0.645 Å) [30].

TGA/DTA curves of the pure and one of the representatives Ni-Cu bi-metal doped sample ($LiNi_{0.03}Cu_{0.03}Mn_{1.94}O_4$) are shown in Figure 4. All the synthesized samples follow the same thermal behavior and showed two step weight losses below 400 ^oC. A slight weight loss (~4%) observed at around 170 ^oC is attributed to the removal of adsorbed moisture due to the hygroscopic nature of the material. The second weight loss between 200 ^oC to 400 ^oC which is also accompanied by a sharp exothermic peak in the DTA curves is due to the combustion of carbonaceous materials from acetate and chelating agents. No weight loss occurs after about 350 ^oC and the TGA curves become flat indicating the phase formation of the pure and doped $LiMn_2O_4$. Elemental composition was measured by ICP-OES analysis. From Table 2 it is evident that Li/Mn/Ni/Cu atomic ratio is very close to the nominal composition.

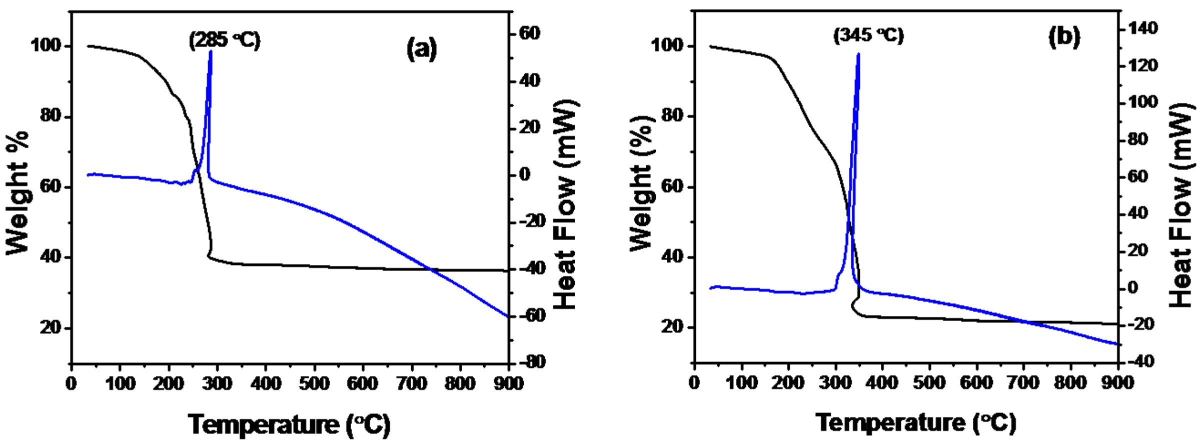

Figure 4.TGA/DTA analysis of(a) $LiMn_2O_4$ (b) $LiNi_{0.03}Cu_{0.03}Mn_{1.94}O_4$

Table 2. Chemical Composition of the pure and Ni-Cu bi-metal doped samples.

No.	Nominal composition	Experimental composition
1	$LiMn_2O_4$	$Li_{0.98}Mn_{1.98}O_4$
2	$LiNi_{0.01}Cu_{0.01}Mn_{1.98}O_4$	$Li_{1.023}Ni_{0.015}Cu_{0.013}Mn_{1.978}O_4$
3	$LiNi_{0.02}Cu_{0.02}Mn_{1.96}O_4$	$Li_{1.011}Ni_{0.025}Cu_{0.023}Mn_{1.958}O_4$
4	$LiNi0_{.03}Cu_{0.03}Mn_{1.94}O_4$	$Li_{1.004}Ni_{0.033}Cu_{0.035}Mn_{1.945}O_4$
5	$LiNi_{0.04}Cu_{0.04}Mn_{1.92}O_4$	$Li_{0.986}Ni_{0.044}Cu_{0.046}Mn_{1.916}O_4$
6	$LiNi_{0.05}Cu_{0.05}Mn_{1.90}O_4$	$Li_{1.042}Ni_{0.049}Cu_{0.054}Mn_{1.897}O_4$

FTIR spectra of the pure and NC-LMO samples are shown in Figure 5. The characteristic peaks observed in the range of 514-620 cm^{-1} are peaks assigned to the stretching vibration of MO_6 octahedral groups in the range [31, 32]. This indicates that low content metal doping has not resulted in any structural change in the $LiMn_2O_4$. However, a minor shift observed in the frequency towards higher wave number depicts the successful Ni-Cu co-doping in the spinel of the metal cations spinel framework. The electrochemical performances of the prepared samples were measured by assembling them into CR2032 coin-type cells with lithium metal as the negative electrode. Cyclic voltammetric measurement was first carried out to understand the electrochemical behavior of the pure and NC-LMO samples at a scan rate of 0.1 mV s^{-1}. As illustrated in Figure 6, there are two pairs of reversible redox peaks at around 4.15/4.10 and 4.03/3.97 V that can be attributed to the two step lithium-ion insertion and extraction reaction of spinel $LiMn_2O_4$. CV curves also illustrate that the redox peaks are well-separated and sharp for the NC-LMO samples which point towards the good stability of the doped spinel framework [33].

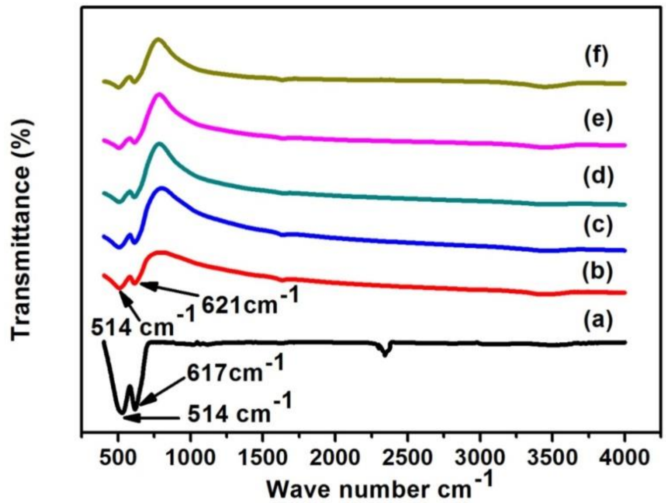

Figure 5. FTIR spectra of (a) $LiMn_2O_4$ (b) $LiNi_{0.01}Cu_{0.01}Mn_{1.98}O_4$ (c) $LiNi_{0.02}Cu_{0.02}Mn_{1.96}O_4$ (d) $LiNi_{0.03}Cu_{0.03}Mn_{1.94}O_4$ (e) $LiNi_{0.04}Cu_{0.04}Mn_{1.92}O_4$ (f) $LiNi_{0.05}Cu_{0.05}Mn_{1.90}O_4$.

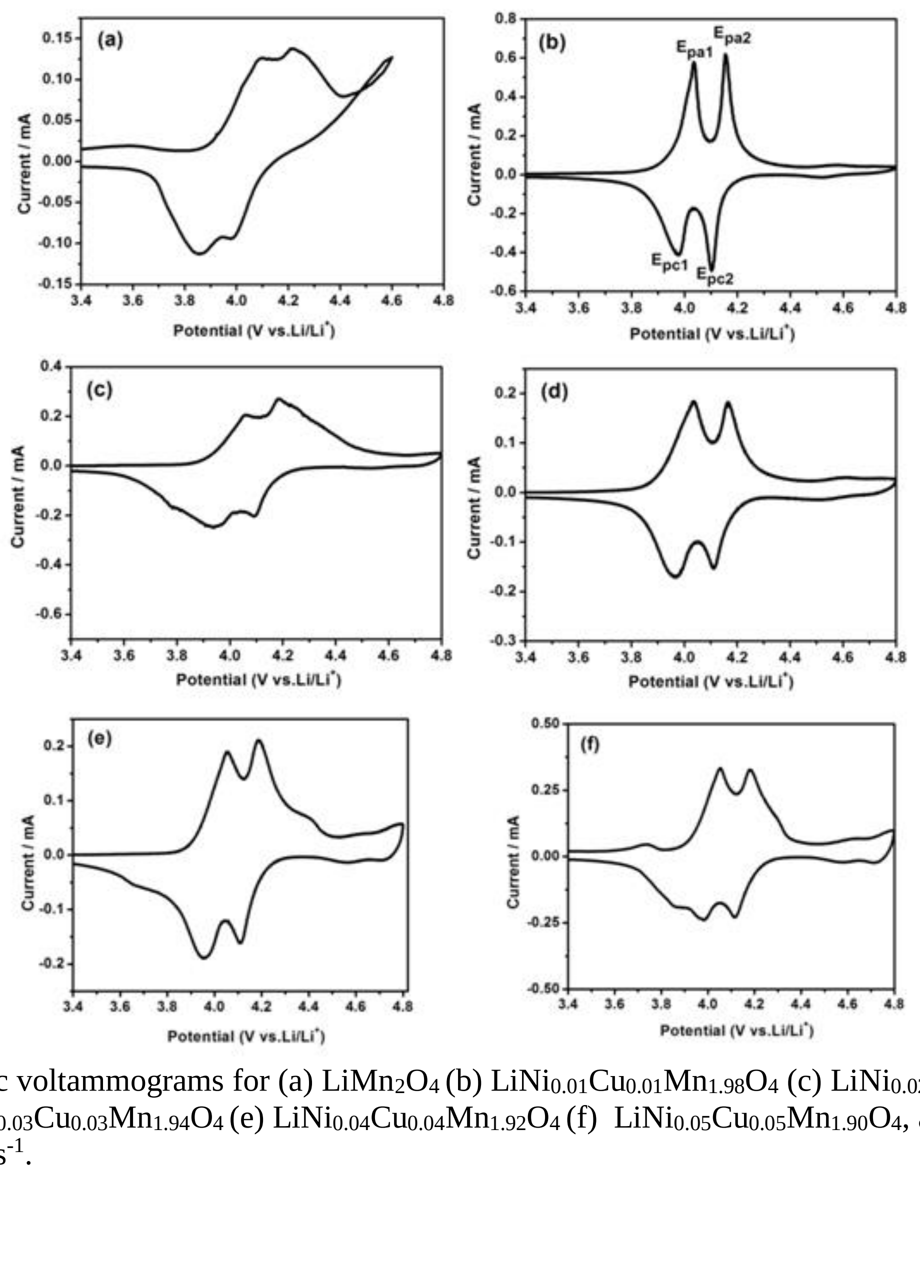

Figure 6. Cyclic voltammograms for (a) $LiMn_2O_4$ (b) $LiNi_{0.01}Cu_{0.01}Mn_{1.98}O_4$ (c) $LiNi_{0.02}Cu_{0.02}Mn_{1.96}O_4$ (d) $LiNi_{0.03}Cu_{0.03}Mn_{1.94}O_4$ (e) $LiNi_{0.04}Cu_{0.04}Mn_{1.92}O_4$ (f) $LiNi_{0.05}Cu_{0.05}Mn_{1.90}O_4$, at a scan rate of 0.1 mV s^{-1}.

Besides the characteristic peaks of $LiMn_2O_4$ at about 4.0 V, two weak split redox peaks at around 4.7 V are also observed for the doped samples with relatively higher amount of the Ni and Cu (i.e., $LiNi_{0.04}Cu_{0.04}Mn_{1.92}O_4$ and $LiNi_{0.05}Cu_{0.05}Mn_{1.90}O_4$). These weak split peaks can be ascribed to reversible Ni^{2+}/ Ni^{4+} redox reactions [34].

Figure7(a) shows the initial discharge curves of the prepared electrode materials between 3.0 and 4.8 V at 0.3 C. It can be seen that all the materials exhibit two voltage plateaus at around 4.1 and 3.9 V that correspond to the two pairs of redox peaks observed in the CV curves [35, 36]. The initial discharge capacities of the NC-LMO electrodes decrease with increasing Ni and Cu contents. The cycling performance of the pure and NC-LMO electrodes is shown in Figure7(b). As can be seen, the pure sample delivered highest 122 mAh g^{-1} initial discharge capacity in the first cycle, but it only retains 72% of the initial discharge capacity after 100 charge/ discharge cycles.

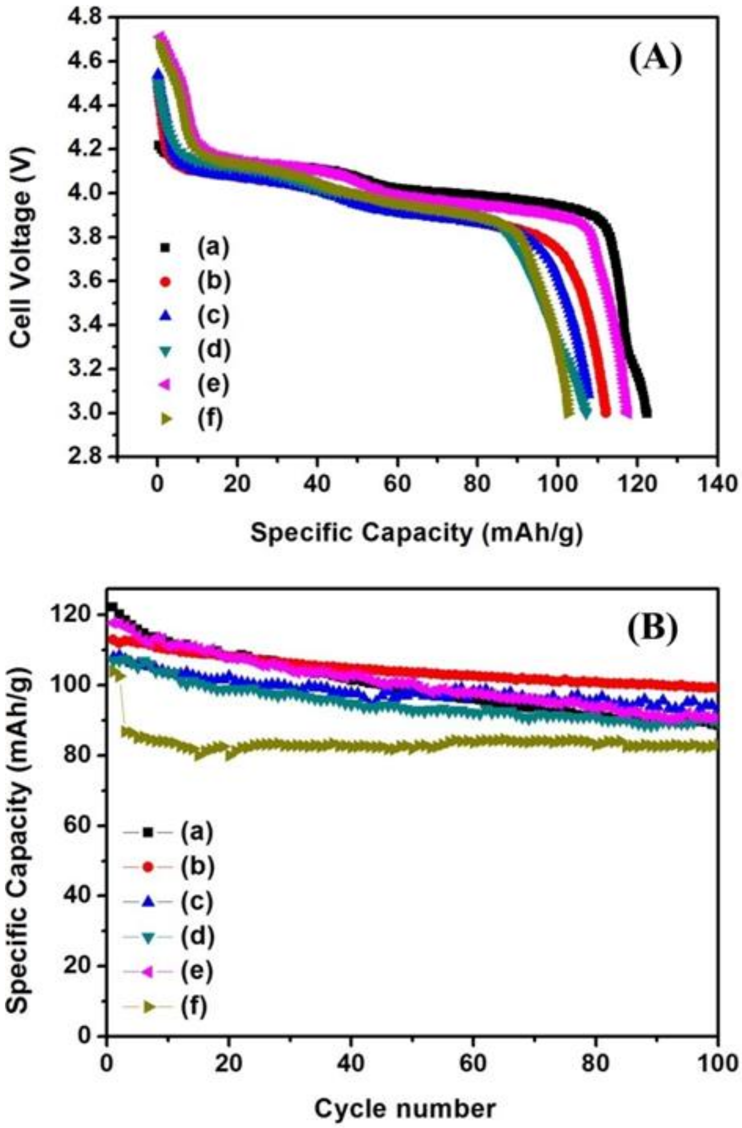

Figure7. (A) First discharge curves, (B) cycling performance of (a)$LiMn_2O_4$ (b) $LiNi_{0.01}Cu_{0.01}Mn_{1.98}O_4$ (c) $LiNi_{0.02}Cu_{0.02}Mn_{1.96}O_4$ (d) $LiNi_{0.03}Cu_{0.03}Mn_{1.94}O_4$ (e) $LiNi_{0.04}Cu_{0.04}Mn_{1.92}O_4$ (f) $LiNi_{0.05}Cu_{0.05}Mn_{1.90}O_4$ at 0.3 C.

On the other hand, NC-LMO cathode materials delivered initial discharge capacities of 113, 108, 107, 118 and 104 mAh g^{-1}. Thus, the capacity retention for the doped samples such as $LiNi_{0.01}Cu_{0.01}Mn_{1.98}O_4$, $LiNi_{0.02}Cu_{0.02}Mn_{1.96}O_4$, $LiNi_{0.03}Cu_{0.03}Mn_{1.94}O_4$, $LiNi_{0.04}Cu_{0.04}Mn_{1.92}O_4$ and $LiNi_{0.05}Cu_{0.05}Mn_{1.90}O_4$, respectively is 88, 86, 83, 77 and 80 %. The above observation indicated that the capacity decrease becomes lower with Ni and Cu co-doping as it has been reported that doping metal cations at the Mn site result in the increase of the average Mn oxidation state and ultimate decrease of the Jahn-Teller distortion which leads to low capacity fading upon repeated charge/ discharge cycling [37]. Detailed comparison of the electrochemical performance for all the prepared electrode materials is shown in Table 3. Among all the investigated Ni-Cu doped samples, NC-LMO sample with the lowest Ni and Cu contents ($LiNi_{0.01}Cu_{0.01}Mn_{1.98}O_4$) shows the best electrochemical performance in terms of initial discharge capacity and excellent cycling performance.

Table 3. Electrochemical performance of the pure and Ni-Cu doped $LiMn_2O_4$ at 0.3 C.

No.	Sample	Specific capacity ($mAhg^{-1}$) at 1st cycle	Specific capacity ($mAhg^{-1}$) after 100 cycles	Capacity Retention (%)
1	$LiMn_2O_4$	122	88	72
2	$LiNi_{0.01}Cu_{0.01}Mn_{1.98}O_4$	113	99	88
3	$LiNi_{0.02}Cu_{0.02}Mn_{1.96}O_4$	108	93	86
4	$LiNi_{0.03}Cu_{0.03}Mn_{1.94}O_4$	107	89	83
5	$LiNi_{0.04}Cu_{0.04}Mn_{1.92}O_4$	118	91	77
6	$LiNi_{0.05}Cu_{0.05}Mn_{1.90}O_4$	104	83	80

Figure 8 shows the rate performance of the pure $LiMn_2O_4$ and $LiNi_{0.01}Cu_{0.01}Mn_{1.98}O_4$ electrodes. The assembled cells for each material were charged at a constate rate of 0.1 C and then discharged at 0.1 C, 0.3 C, 0.5 C, 1 C, 2 C and 5 C values between 3.0-4.8 V. It can be seen that samples remain stable and the specific capacity decrease steadily as the C-rate increases. Although at 0.1 and 0.3 C, the specific discharge capacity of the pure $LiMn_2O_4$ is slightly higher than $LiNi_{0.01}Cu_{0.01}Mn_{1.98}O_4$.

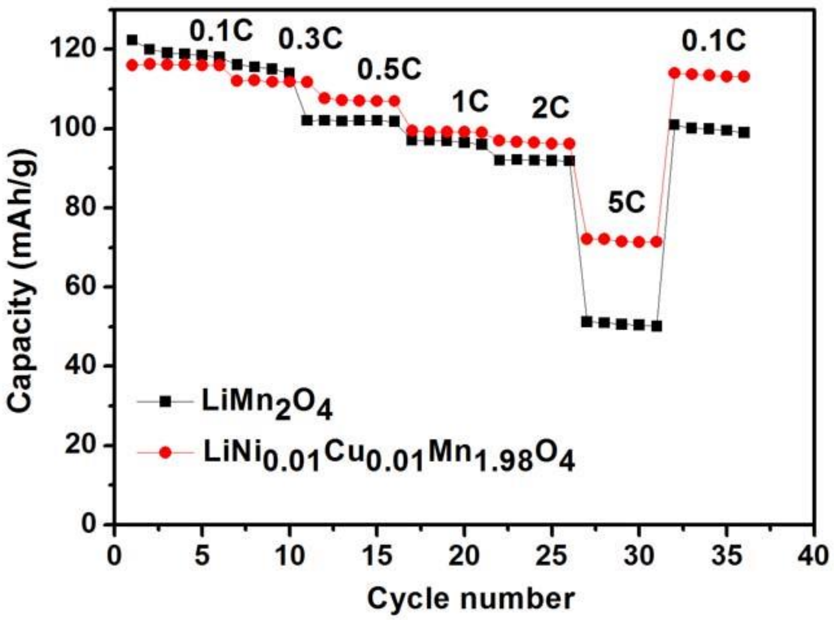

Figure 8. Rate capability of the pure $LiMn_2O_4$ and $LiNi_{0.01}Cu_{0.01}Mn_{1.98}O_4$.at different rates.

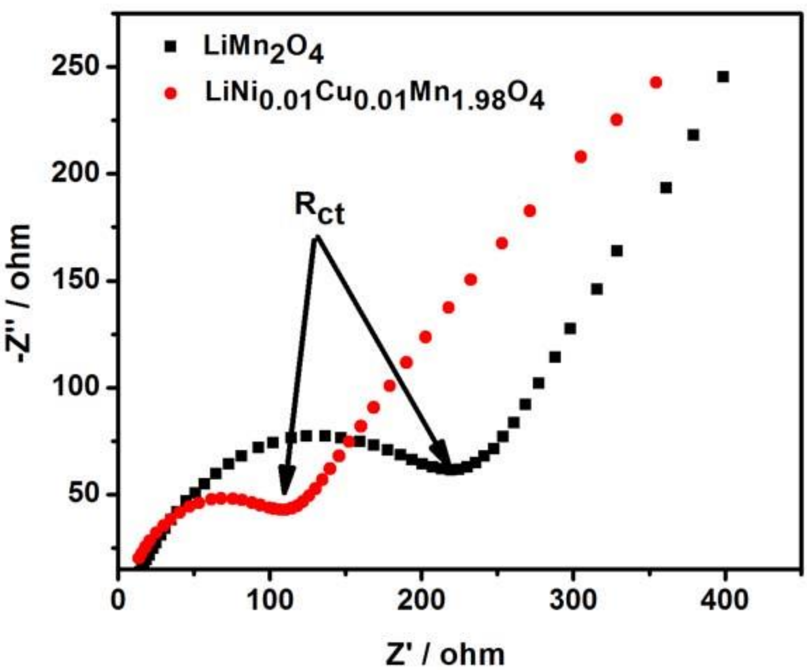

Figure 9. Electrochemical impedance spectra of the pure $LiMn_2O_4$ and $LiNi_{0.01}Cu_{0.01}Mn_{1.98}O_4$.

However, the high rate performance of $LiNi_{0.01}Cu_{0.01}Mn_{1.98}O_4$ electrode exceeds pure $LiMn_2O_4$ sample. Moreover, $LiNi_{0.01}Cu_{0.01}Mn_{1.98}O_4$ exhibits relatively higher specific capacities after 10 charge/ discharge cycles at high C-rates. From Figure 8, it can also be found that after deep cycling at higher rate (5 C) when the current rate was reduced back to 0.1 C, $LiNi_{0.01}Cu_{0.01}Mn_{1.98}O_4$ delivers 114 mAh g^{-1} discharge capacity which is 98 % of the initial discharge capacity in the 1st cycle. As a comparison the discharge capacity of the pure $LiMn_2O_4$ sample recovers to 101 mAh g^{-1} after 30 cycles at 0.1 C and the capacity retention is about 82%. The above results indicated that the spinel framework became more tolerant and robust to the repeated charge/ discharge cycling by Ni and Cu bi-metal doping.

In order to better understand the charge transfer kinetics, electrochemical impedance spectroscopy (EIS) measurement was performed. Nyquist plots of the pure $LiMn_2O_4$ and $LiNi_{0.01}Cu_{0.01}Mn_{1.98}O_4$ samples are shown in Figure 9. $LiNi_{0.01}Cu_{0.01}Mn_{1.98}O_4$ sample shows much lower charge transfer resistance (~97 Ω) than the pure sample (~212 Ω). This indicates that doping spinel $LiMn_2O_4$ with low content of Ni and Cu obviously increases Li-ion conductivity that resulted in enhanced cycling performance [38].

Table 4. Comparison of electrochemical performance of various transition metal doped $LiMn_2O_4$

Sample	1st dis. capacity (mAhg^{-1}) / C-rate	Dis.cap (mAhg^{-1}) @No. of cycles/ C-rate	Capacity retention (%)	Reference
$LiNi_{0.01}Cu_{0.01}Mn_{1.98}O_4$	113/0.3C	99@100/0.3C	88	This work
$LiZn_{0.1}Pr_{0.1}Mn_{1.80}O_4$	130/0.1C	114@10/0.1C	88	[39]
$LiCr_{0.5}Mg_{0.05}Mn_{1.45}O_4$	123/0.1C	114.4@10/0.1C	93	[40]
$LiCu_{0.5}Al_{0.05}Mn_{1.45}O_4$	120/0.1C	115.2@10/0.1C	95	[41]
$Li_{1.02}Co_{0.1}Ni_{0.1}Mn_{1.98}O_4$	118/0.3C	109@40/0.3C	92	[42]
$LiCr_{0.1}Mn_{1.90}O_4$	138/0.1C	100@10/0.1C	72	[43]
$LiMn_{1.98}Dy_{0.02}O_4$	122/0.1C	104@10/0.1C	85	[44]

The electrochemical performance of $LiNi_{0.01}Cu_{0.01}Mn_{1.98}O_4$ is compare to or even better to that of many transition metal doped $LiMn_2O_4$ (Table 4). Capacity retention of $LiNi_{0.01}Cu_{0.01}Mn_{1.98}O_4$ after 100 cycles at 0.3C is superior to other reported work [39-44].

The better electrochemical performance of $LiNi_{0.01}Cu_{0.01}Mn_{1.98}O_4$ among all the synthesized samples can be attributed to the lower Jahn-Teller distortion effect that provides chemical and structural stabilization, more uniform and low agglomerated nanoparrticles, low charge transfer resistance (as evident from EIS measurement) and possibly high erelectronic conductivity provided by coppper doping as well as large binding energies of the doped cations.

4. CONCLUSIONS

Low content Ni and Cu substitution of spinel $LiMn_2O_4$ framework has been found to notably improve the charge/ discharge cycling and high rate performance. Specifically, $LiNi_{0.01}Cu_{0.01}Mn_{1.98}O_4$ delivered initial discharge capacity of 113 mAh g^{-1} at 0.3 C with 88% capacity retention after 100 charge/ discharge cycles. Moreover, after deep cycling at higher rate of 5 C when the current rate was reduced back to 0.1 C, $LiNi_{0.01}Cu_{0.01}Mn_{1.98}O_4$ delivers 114 mAh g^{-1}discharge capacity which is 98 % of the initial discharge capacity in the 1st cycle. The better electrochemical performance of NC-LMO samples compared to the pure $LiMn_2O_4$ may be attributed to the suppression of the Jahn-Teller distortion, low Mn dissolution, more uniform particle size and low charge transfer resistance. The study demonstrates that Ni and Cu bi-metal doping is beneficial for the improved electrochemical performance of high voltage cathode materials for lithium-ion rechargeable batteries.

ACKNOWLEDGEMENTS
This work was financially supported by the National R&D Program of China (2016YFB0100301) and National 863 Program of China (2015AA034601).

References

1. K. Kang, Y.S. Meng, J. Bréger, C.P. Grey, G. Ceder, *Science*, 311 (2006) 977.
2. M. S. Whittinghm, *Chem. Rev*., 104 (2004) 4271.
3. V. Etacheri, R. Marom, R. Elazari, G. Salitra, D. Aurbach, *Energy Environ. Sci*., 4 (2011) 3243.
4. B. Scrosati, J. Hassoun, Y.K. Sun, *Energy Environ. Sci*., 4 (2011) 3287.
5. M. Armand, J.M. Tarascon, *Nature*, 451(2008) 652.
6. B. Dunn, H. Kamath, J.M. Tarascon, *Science*, 334 (2011) 928.
7. M. S. Whittingham, *Science*,192 (1976) 1126.
8. J. Liu, P. Kopold, C. Wu, P.A. Van Aken, J. Maier, Y. Yu, *Energy Environ. Sci*., 8 (2015) 3531.
9. J. Liu, Y. Wen, Y. Wang, P.A. Van Aken, J. Maier, Y. Yu, *Adv. Mater*., 26 (2014) 6025.
10. J. Liu, Y. Wen, Y. Wang, P.A. Van Aken, J. Maier, Y. Yu, *Nano Lett*., 14 (2014) 6387.
11. M. Thackeray, P. Johnson, L. De Picciotto, P. Bruce, J. Goodenough, *Mater. Res. Bull*., 19 (1984) 179.
12. M. Thackeray, A. De Kock, *J. Solid State Chem*., 74 (1988) 414.
13. M. Jayalakshmi, M. Mohan Rao, F. Scholz, *Langmuir*, 19 (2003) 8403.
14. J. Cabana, T. Valdés-Solís, M. Palacín, J. Oró-Solé, A. Fuertes, G. Marbán, A. Fuertes, *J. Power Sources*, 166 (2007) 492.
15. J.Y. Luo, Y.G. Wang, H.-m. Xiong, Y.-y, Xia, *Chem. Mater*., 19 (2007) 4791.
16. H.K. Song, K.T. Lee, M.G. Kim, L.F. Nazar, J. Cho, *Adv. Funct. Mater*., 20 (2010) 3818.
17. F. Wu, N. Li, Y. Su, H. Shou, L. Bao, W. Yang, L. Zhang,R. An, S. Chen, *Adv. Mater*., 25 (2013) 3722.
18. M.-J. Lee, S. Lee, P. Oh, Y. Kim, J. Cho, *Nano Lett*., 14 (2014) 993.
19. P.G. Bruce, B. Scrosati, J.M. Tarascon, *Angew. Chem., Int. Ed*., 47 (2008) 2930.
20. X. Zhao, M. Reddy, H. Liu, S. Ramakrishna, G.S. Rao, B.V. Chowdari, *RSC Adv*., 2 (2012) 7462.
21. R. Gummow, A. De Kock,M. Thackeray, *Solid State Ion*., 69 (1994) 59.
22. Q. Zhong, A. Bonakdarpour, M. Zhang, Y. Gao, J. Dahn, *J. Electrochem.Soc*., 144 (1997) 205.
23. Y. J. Lee, S.-H. Park, C. Eng, J. B. Parise, C. P. Grey, *Chem. Mater*., 14 (2002) 194.
24. Y. Ding,J. Xie,G. Cao,T. Zhu,H. Yu, X. Zhao, *J. Phy. Chem.C*., 115 (2011) 9821.
25. W. Fu-Cheng, T. Jian-Kun, Z. Hai-Lang, *Int. J. Electrochem. Sci.*, 9 (2014) 4627.
26. A. Iqbal, Y. Iqbal, L. Chang, S. Ahmed, Z. Tang, Y. Gao, *J. Nanopart. Res*., 14 (2012) 1-14.
27. F. Wang, J. Wang, H. Ren, H. Tang, R. Yu, D. Wang, *Inorg. Chem. Front*., 3 (2016) 365.
28. Y.-S. Lee, Y.-K. Sun, K.-S. Nahm, *Solid State Ionics*, 109 (1998) 285.
29. R.D. Shannon, *Acta Crystallogr., Sect. A*, 32 (1976) 751.
30. M.-C. Yang, B. Xu, J.-H. Cheng, C.-J. Pan, B.-J. Hwang, Y.S. Meng, *Chem. Mater*., 23 (2011) 2832.
31. C. Wu, Z. Wang, F. Wu, L. Chen, X. Huang, *Solid State Ionics*, 144 (2001) 277.
32. B. Ammundsen,G.R. Burns, M.S. Islam, H. Kanoh, J. Rozière, *J. Phys. Chem. B*, 103 (1999) 5175.
33. B.-L. He, W.-J. Zhou, Y.-Y. Liang, S.-J. Bao, H.-L. Li, *J. Colloid Interface Sci*., 300 (2006) 633.
34. T.-F. Yi, J. Shu, Y.-R. Zhu, R.-S. Zhu, *J. Phys. Chem. Solids*, 70 (2009) 153.
35. L. He, S. Zhang, X. Wei, Z. Du, G. Liu, Y. Xing, *J. Power Sources*, 220 (2012) 228.

36. L. Xiao, Y. Zhao, Y. Yang, Y. Cao, X. Ai, H. Yang, *Electrochim. Acta*, 54 (2008) 545.
37. C. Shen, R. Liu, R. Gundakaram, J. Chen, S. Huang, J. Chen, C. Wang, *J. Power Sources*, 102 (2001) 21.
38. R.-H.Zeng, W.-s. Li, L. Dong-sheng, Q.-M. Huang, L.-Z. Zhao, *Trans. Nonferrous Met. Soc. China*, 17 (2007) 1312.
39. R. Thirunakaran, J. Sol-Gel Sci. Technol., 69 (2014) 397.
40. R. Thirunakaran, G. H. Lew, W. S. Yoon, *J. Powtec*. 301 (2016) 197.
41. R. Thirunakaran, G. H. Lew, W. S. Yoon, *J. Electroanal. Chem*. 767 (2016) 141.
42. B. J. Hwang, R. Santhanam, S. G. Hu, *J. Power Sources*, 108 (2002) 250.
43. R. Thirunakaran, A. Sivashanmugam , S. Gopukumar, C. W. Dunnill, D. H. Gregory, *Mater. Res. Bull*., 43 (2008) 2119.
44. P. Ram, R. Singhal, G. Choudhary , R. K. Sharma, *J. Electroanal. Chem*. 802 (2017) 94.